PROCEEDINGS of the
23rd International Congress on Acoustics

9 to 13 September 2019 in Aachen, Germany

Design of acoustic partitions with thin plate-like acoustic metamaterials

Felix LANGFELDT[1]; Wolfgang GLEINE[2]
Hamburg University of Applied Sciences, Germany

ABSTRACT

Acoustic metamaterials have emerged as new means for sound control with extraordinary properties, such as negative effective density and/or bulk modulus. Amongst the variety of different realizations of acoustic metamaterials, thin plate-like metamaterials (e.g. membrane-type acoustic metamaterials or inhomogeneous plates) have a high potential for improving the sound transmission loss of conventional partitions, especially in the challenging low-frequency regime. These types of metamaterials have been previously shown to achieve very high sound transmission loss values which can exceed the corresponding mass-law values considerably. However, further investigations have shown that when these metamaterials are integrated into a double wall partition, the beneficial effect of the metamaterials can be greatly diminished if an improper design is chosen. This contribution aims at providing a more detailed understanding of the important parameters in the design of acoustic partitions with thin plate-like acoustic metamaterials. The metamaterial is represented by a simple black-box model in order to reduce the parameter space. Analytical calculations of combinations of the metamaterial with single and double walls are used to identify the most relevant design parameters and possible limitations in the acoustic performance. General design guidelines for acoustic partitions are derived from these results and applied to laboratory test samples.

Keywords: acoustic metamaterial, glass wool, transmission loss, plate

1. INTRODUCTION

The emergence of the so-called acoustic metamaterials 20 years ago has opened up new possibilities for controlling the propagation of sound. The term acoustic metamaterials stands for composite structures composed of periodically arranged unit cells for the systematic manipulation of the effective parameters for sound waves. Many different realizations of acoustic metamaterials exhibiting negative density or bulk modulus (and even both simultaneously) have been investigated thoroughly enabling new applications, such as acoustic cloaks and perfect acoustic lenses (1). Amongst the many different kinds of acoustic metamaterials, the plate-like acoustic metamaterials (PAM) are of particular interest in applications of low-frequency noise control. PAM are thin two-dimensional metamaterials exhibiting frequency bands at low frequencies with negative density and—compared to the mass law—considerably enhanced sound transmission loss (STL). These properties make PAM promising candidates for applications in noise control engineering where mass and installation space of noise reduction means are highly constrained (e.g. automotive or aeronautical engineering).

One of the first realizations of PAM, the so-called membrane-type acoustic metamaterials, were published by Yang et al. (2). They and subsequent publications demonstrated that these metamaterials, consisting of subwavelength sized unit cells with a thin prestressed membrane and small attached masses, can achieve narrowband anti-resonances with STL values much higher than the corresponding mass law. Similar to the membrane-type PAM are plates with periodically added masses, which have been investigated already in the 1950s by Kurtze (3) and have been recently rediscovered in the context of acoustic metamaterials for enhanced low-frequency sound insulation (4, 5). Contrary to the membrane-type PAM, these metamaterials do not require a relatively stiff grid structure to subdivide the plate into individual unit cells and still exhibit low-frequency anti-resonances with highly improved STL. Xiao et al. (6) investigated another type of PAM, where spring-mass resonators were distributed periodically on a plate and the STL of the plate could be considerably improved at the resonance frequencies of the attached resonators. Claeys et al. (7) applied this concept to an additively manufactured metamaterial enclosure with periodically embedded resonators to achieve a relatively broadband sound reduction below 1 kHz.

[1] Felix.Langfeldt@haw-hamburg
[2] Wolfgang.Gleine@haw-hamburg.de

All these different PAM designs have been shown to exhibit large low-frequency STL values when the transmission of sound is considered through the metamaterial only. However, in many applications it could be required to combine the metamaterials with conventional acoustic partitions, such as walls. One example for this is the aircraft sidewall, where the fuselage structure and the interior lining panels result in a double wall-like arrangement. Previous studies of the performance of membrane-type acoustic metamaterials in the air gap of a double wall have shown that the anti-resonance effect of the metamaterial depends highly on the position of the metamaterial within the double wall (8). In the worst case, the STL improvement of the metamaterial can be nullified by additional resonances appearing in the multi-layered structure. While in Ref. (8) it was concluded that the optimal placement of the PAM inside the double wall was as close to one wall as possible, it remained inconclusive if this could be generalized to other double wall configurations as well. In Ref. (9) it was shown that the STL of a double wall can be greatly improved at the mass-air-mass resonance frequency by replacing one of the walls by a PAM with periodically attached resonators tuned to the mass-air-mass resonance frequency. However, in some applications it might be necessary to tune the anti-resonances of the PAM to other frequencies than the mass-air-mass resonance. In this case, it can be expected that the performance of the PAM can be also significantly reduced if an improper design is chosen.

The objective of this contribution is to provide a more general understanding of the acoustical properties of partitions with additional PAM layers for the improvement of low-frequency sound insulation. In Section 2, a generalized model for PAM using the effective surface mass density representation with a simple two degrees of freedom (2DOF) model is presented. This black-box model is able to represent a wide range of different PAM designs using only a small set of parameters. It is employed in Section 3 to investigate the acoustic interactions of a PAM in combination with single and double walls. The paper is concluded in Section 4 with a summary of the findings and general recommendations for the design of acoustic partitions with PAM.

2. GENERALIZED MODEL FOR PLATE-LIKE ACOUSTIC METAMATERIALS

This section provides a generalized model to represent most PAM types with only a small set of easily determinable parameters. First, Section 2.1 describes the effective mass representation used for the PAM modeling. Then, the transfer matrix model used for modeling multi-layered partitions with PAM is described briefly. The models are validated in Section 2.3 using simulations and experiments.

2.1 Effective mass representation

Since, typically, the PAM are very thin compared to the acoustic wavelength, they can be represented as a slab with a frequency-dependent effective surface mass density m''_{eff}. For the purpose of this contribution, the PAM considered here are characterized by a single anti-resonance (with greatly increased effective surface mass density) followed by a resonance (with near-zero m''_{eff}). Thus, the following 2DOF representation for m''_{eff} can be used:

$$m''_{\mathrm{eff}}(\omega) = m''_0 \frac{|p|^2(z - \mathrm{i}\omega)(z^* - \mathrm{i}\omega)}{|z|^2(p - \mathrm{i}\omega)(p^* - \mathrm{i}\omega)}, \tag{1}$$

where m''_0 is the static surface mass density of the PAM and z and p are the complex zero and pole of the PAM, respectively. These are given by

$$z = \mathrm{i}2\pi f_{\mathrm{R}}\left(\sqrt{1-\zeta_{\mathrm{R}}^2} + \mathrm{i}\zeta_{\mathrm{R}}\right) \quad \text{and} \quad p = \mathrm{i}2\pi f_{\mathrm{P}}\left(\sqrt{1-\zeta_{\mathrm{P}}^2} + \mathrm{i}\zeta_{\mathrm{P}}\right), \tag{2}$$

with the resonance frequency f_{R}, anti-resonance frequency f_{P}, and the corresponding modal damping ratios ζ_{R} and ζ_{P}. In the undamped case, $\zeta_{\mathrm{R}} = \zeta_{\mathrm{P}} = 0$ and Eq. (1) reduces to

$$m''_{\mathrm{eff}}(f) = m''_0 \frac{1 - f^2/f_{\mathrm{R}}^2}{1 - f^2/f_{\mathrm{P}}^2}. \tag{3}$$

Similar formulations to Eqs. (1) and (3) have been used previously to characterize the effective material properties of PAM (e.g. (6, 9)). The advantage of these models is that every PAM design can be represented by Eq. (1) with only five parameters which are relatively easy to determine using experimental, numerical, or analytical methods. In the undamped case of Eq. (3) it is even sufficient to determine only three parameters (the PAM mass and the two characteristic frequencies) to fully describe the dynamic behavior of the PAM at low frequencies. On the other hand, Eq. (1) can also be interpreted as a black-box model which enables the design of acoustic partitions with PAM using quantities like mass, (anti-)resonance frequencies, and damping before any specific PAM designs are chosen. Once eligible values for these parameters have been determined, the PAM can be designed specifically for achieving these design parameters.

2.2 Transfer matrix model

In order to estimate the STL of multi-layered acoustic partitions with PAM, the transfer matrix method is employed. A 2-by-2 transfer matrix $\mathbf{T}$ relates the acoustic pressure and particle velocity on both sides of a laterally infinite layer (e.g. an air gap or a wall) and can be easily calculated for multi-layered partitions by multiplying the transfer matrices of all layers (10). The four elements T_{11}, T_{12}, T_{21}, and T_{22} of a transfer matrix can be used to calculate the characteristic acoustic quantities of the partition, such as the sound transmission loss TL. For common layers, such as air layers and porous absorber blankets, analytical expressions for the transfer matrices can be found in the literature (e.g. (10, pp. 244–257)). In the case of an acoustically thin slab, the transfer matrix can be expressed in terms of the wall impedance Z_w as

$$\mathbf{T}_\mathrm{w} = \begin{bmatrix} 1 & Z_\mathrm{w}(\omega) \\ 0 & 1 \end{bmatrix}. \tag{4}$$

For a limp wall with surface mass density m'', the wall impedance is given by $Z_\mathrm{w}(\omega) = \mathrm{i}\omega m''$. For the modeling of a PAM layer, the wall impedance is obtained in the same form but with m'' replaced by the effective surface mass density given in Eq. (1), i.e. $Z_\mathrm{w}(\omega) = \mathrm{i}\omega m''_\mathrm{eff}(\omega)$ (8).

2.3 Validation

The modeling approach for acoustic partitions with PAM presented in this section is first validated using finite element model (FEM) simulations for two different types of PAM designs. Then, experimental results for a plate model with a PAM layer under diffuse field excitation are presented to validate the transfer matrix model.

Figure 1(a) shows the simulated normal incidence sound transmission loss TL of a periodic PAM unit cell consisting of a thin film with an attached ring mass (similar to the PAM investigated in Ref. (5)). The edge boundary conditions of the unit cell were periodic in order to simulate a laterally unbounded metamaterial plate. The film material was a 100 µm thick PET film (density $\rho = 1570\,\mathrm{kg/m^3}$, Young's modulus $E = 4.7\,\mathrm{GPa}$, Poisson's ratio $\nu = 0.4$, and structural loss factor $\eta = 10\,\%$) and the dimensions of the unit cell were given by $35\,\mathrm{mm} \times 35\,\mathrm{mm}$. The polyamide ring mass was $t_\mathrm{M} = 1.6\,\mathrm{mm}$ thick with an outer and inner diameter of $d_\mathrm{M,o} = 18\,\mathrm{mm}$ and $d_\mathrm{M,i} = 6.4\,\mathrm{mm}$, respectively, resulting in an added mass of $M = 0.39\,\mathrm{g}$. Thus, the static surface mass density of this PAM is comparatively low with $m''_0 = 0.48\,\mathrm{kg/m^2}$. For the analytical modelling using the 2DOF model in Eq. (1), the characteristic frequencies f_P and f_R as well as the corresponding damping ratios are provided in Table 1. It should be noted that, for simplicity, the damping ratios have been determined by $\zeta_\mathrm{P} = \zeta_\mathrm{R} = 2\eta$.

The analytical and numerical results in Fig. 1(a) exhibit an excellent agreement up to the resonance frequency of the metamaterial $f_\mathrm{R} = 320\,\mathrm{Hz}$. At higher frequencies, the numerical results indicate a second-order anti-resonance at around 700 Hz which the 2DOF model cannot reproduce because Eq. (1) only includes one anti-resonance of the PAM. However, Eq. (1) can in principle be readily extended to include higher-order poles and zeros. Nevertheless, for the analysis of multi-layered partitions with PAM in Section 3 as well as in many practical applications of PAM it suffices to consider only the first anti-resonance of the metamaterial.

Figure 1(b) shows the numerical and analytical STL results of a considerably different PAM design consist-

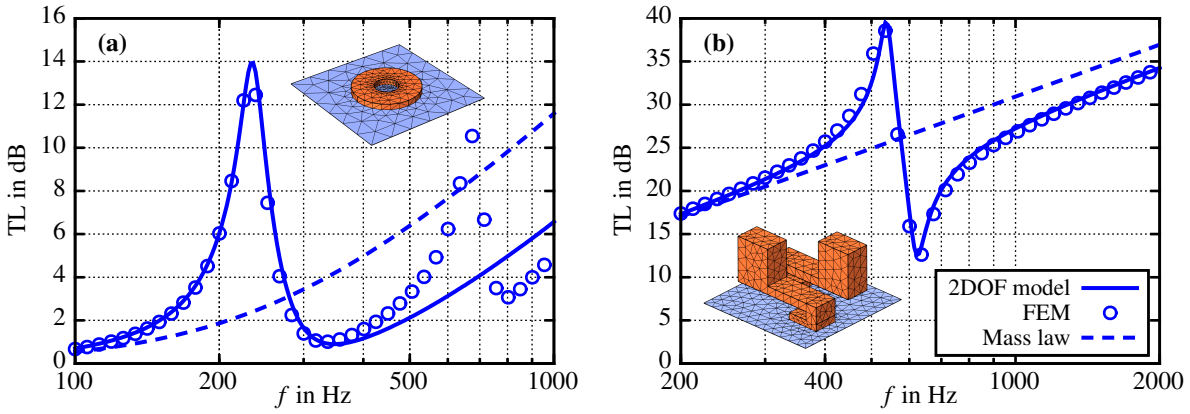

Figure 1 – Numerical and analytical results using the 2DOF model for the normal incidence sound transmission loss TL of two different PAM designs. (a) Thin film with added masses; (b) Plate with micro-resonators (unit cell design from Ref. (9)).

Table 1 – 2DOF model parameters of the different investigated PAM configurations

Configuration	m''_0	f_P	ζ_P	f_R	ζ_R
Film with ring masses (Fig. 1(a))	0.48	235	20	320	20
Plate with micro-resonators (Fig. 1(b))	4.61	539	10	620	10
PAM for plate model (Fig. 2(b))	0.43	390	60	585	60
	kg/m^2	Hz	%	Hz	%

ing of a plate with attached micro resonators. The geometrical and material specifications of this metamaterial are given in Ref. (9). The resulting parameters for the 2DOF model are provided in Table 1. It can be seen that this metamaterial is nearly ten times heavier than the one shown in Fig. 1(a). Therefore, the TL values of this PAM are considerably higher. The agreement between the analytical and numerical results is again excellent. Since for this PAM no higher-order anti-resonance is present within the frequency range of interest, the good agreement extends over all frequencies shown in Fig. 1(b).

It therefore can be concluded that the proposed 2DOF model is capable of representing many different PAM designs using only five parameters for frequencies up to the second- and higher-order (anti-)resonances of the metamaterial unit cell.

An experimental validation of the transfer matrix model for multi-layered partitions with PAM was conducted in the acoustic laboratory of the Hamburg University of Applied Sciences using a 50 cm × 50 cm plate model. The diffuse field sound transmission loss $\mathrm{TL_{diff}}$ was measured according to ISO 15186-1 by mounting the sample inside a transmission window in between a reverberation chamber and a hemi-anechoic room (see Fig. 2(a)) and measuring the transmitted sound power with a sound intensity probe. As shown in Fig. 2(c), the sample consists of a baseplate which is composed of a 3 mm thick MDF plate with a 25 mm layer of lightweight glass wool on top. The surface mass density of this baseplate was measured at $m'' = 2.85\,\mathrm{kg/m^2}$. A PAM made up of a PET film with 169 polyamide ring masses is attached to the transmission window frame using tape (see Fig. 2(b)) with a distance of 50 mm measured from the MDF plate. The surface mass density of the PAM was given by $m''_0 = 0.43\,\mathrm{kg/m^2}$ which is only 15 % of the baseplate mass.

In the analytical model using the transfer matrix method, the MDF plate was modelled as a limp wall with its surface mass density of $2.7\,\mathrm{kg/m^2}$. The glass wool layer was represented by an equivalent fluid model (11) with a limp frame approximation (10, pp. 252-253) using the material parameters density $\rho = 6\,\mathrm{kg/m^3}$, porosity $\phi = 0.99$, and static flow resistivity $\sigma = 19\,\mathrm{kNs/m^4}$. For the PAM layer, the 2DOF model with the parameters provided in Table 1 was used. The diffuse field sound transmission loss of the finite sized test sample was calculated with the resulting transfer matrices using the spatial windowing method by Bonfiglio et al. (12).

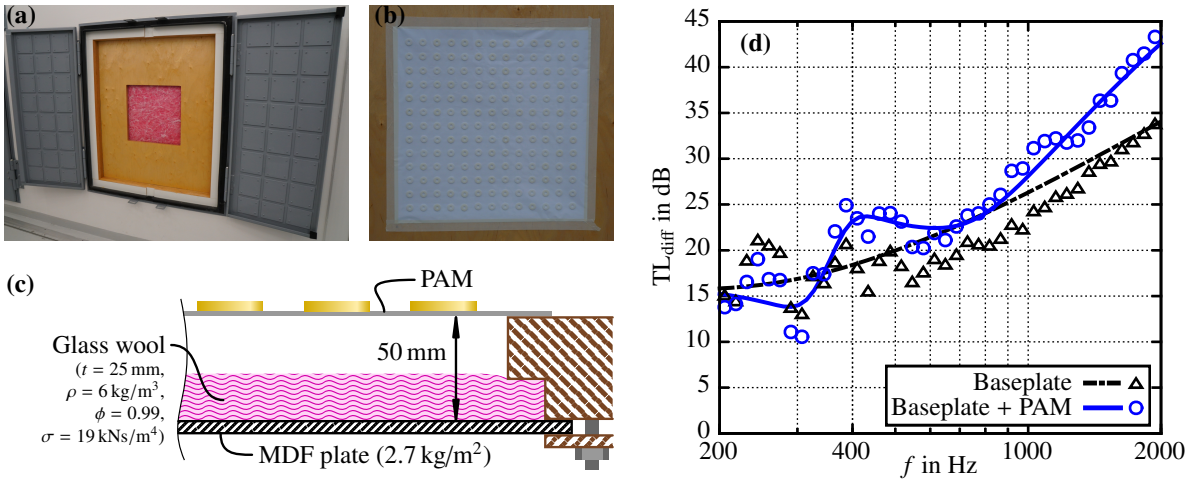

Figure 2 – Experimental and analytical results for the multi-layered partition consisting of a plate, glass wool, and PAM. (a) MDF plate with glass wool inside the transmission window frame; (b) Metamaterial film with ring masses; (c) Schematical drawing of the layering structure; (d) Measured (symbols) and analytically calculated (lines) diffuse field sound transmission loss $\mathrm{TL_{diff}}$.

Figure 2(d) shows the experimental and analytical results for the baseplate (black symbols and lines) and the baseplate with additional PAM layer (blue symbols and lines). In general, a reasonably good agreement between the measured and the calculated data can be observed. It should be noted that at frequencies below 500 Hz the experimental results exhibit strong variations while the analytical results are comparatively smooth. A possible explanation for this could be the modal behavior of the plates and/or the laboratory environment in this frequency range, which is neglected in the analytical model. Verifying this assumption is part of ongoing work. Nevertheless, despite the comparatively simple modeling of the partition, the analytical model yields a good representation of the experimental data. For both analytical and experimental results a considerable improvement of the STL of the baseplate (approximately +6 dB) can be observed around the PAM anti-resonance at $f_P = 390$ Hz. This STL improvement is much higher than what would be expected due to the added mass of the PAM alone (+1.2 dB). Furthermore it can be seen that the STL of the baseplate with PAM improves significantly at frequencies above approximately 700 Hz. This can be explained by the double wall effect which becomes prominent at higher frequencies for this multi-layered partition. Using the surface mass densities of the baseplate and the PET film without masses (which governs the sound transmission through the PAM above f_R), the mass-air-mass resonance frequency of the double wall structure can be estimated at 690 Hz. This frequency is very close to the onset of STL improvement in Fig. 2(d) and therefore gives a strong indication for the importance of the double wall effect in this frequency range.

3. MULTI-LAYERED PARTITIONS WITH PAM

In this section, the analytical model from Section 2 is used to study in more detail the acoustic properties of multi-layered acoustic partitions with PAM. First, a parametric study of the STL of a single wall with an additional PAM layer is performed. Then, in Section 3.2, this study is extended to a double wall with integrated PAM.

3.1 Single wall with PAM

The basic setup of a single wall with PAM is shown schematically in Fig. 3(a). The wall is characterized by a surface mass density m''_{w1} and the PAM is now represented as an acoustically thin layer with frequency-dependent surface mass density $m''_{eff}(f)$ following Eq. (1). The distance between the wall and the PAM is denoted by d_{w1}. Baseline parameters for the single wall with PAM design investigated in this section are given in Table 2.

The acoustic performance of the partition is quantified in terms of the relative +5 dB-bandwidth BW_{+5} (in %). The +5 dB-band is defined as the frequency range for which the normal incidence STL of the wall with PAM is at least 5 dB higher than the STL of the wall alone. The relative bandwidth can be calculated using $BW_{+5} = (f_l - f_u)/\sqrt{f_l f_u}$, where f_l and f_u are the lower and upper limiting frequencies of the +5 dB-band, respectively. The results in Fig. 3(b) are shown as contour lines for a variation of the PAM-wall spacing d_{w1} and the relative PAM resonance frequency f_R/f_P. The reason for choosing these parameters in the variation is that in typical applications the position of the PAM in front of the wall and the PAM resonance frequency

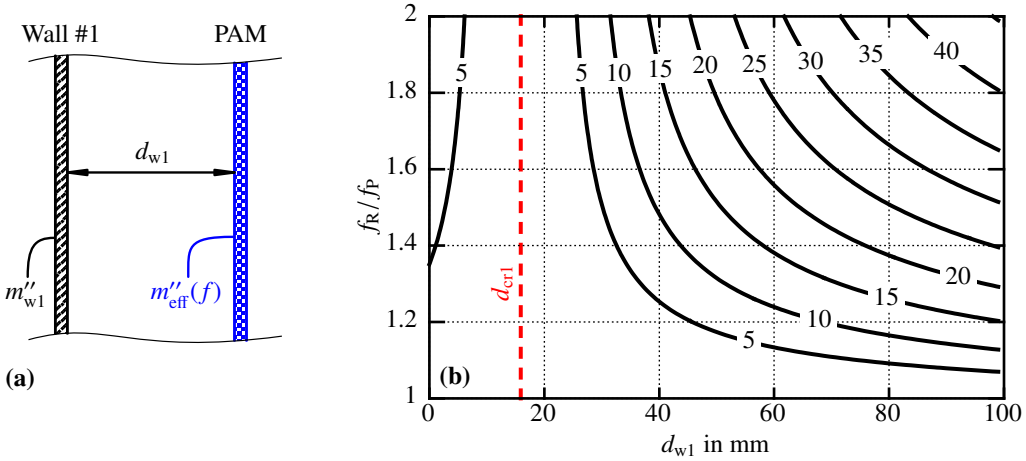

Figure 3 – Sound insulation performance of a single wall with PAM layer. (a) Schematical representation of the configuration; (b) +5 dB-bandwidth (in %) for different PAM-wall spacings d_{w1} and relative PAM resonance frequencies f_R/f_P (baseline parameters given in Table 2).

Table 2 – Baseline parameters for the single and double wall configurations with PAM

Configuration	m''_{w1}	m''_{w2}	H	m''_0	f_P	ζ_P	f_R	ζ_R
Single wall + PAM	2.5	—	—	0.4	300	10	510	10
Double wall + PAM	2.5	1.5	150	0.4	300	10	510	10
	kg/m^2	kg/m^2	mm	kg/m^2	Hz	%	Hz	%

can be chosen more freely than other parameters, such as the additional mass or the anti-resonance frequency, which are more or less fixed by requirements.

In Fig. 3(b) it can be seen that a large value of f_R/f_P leads to higher bandwidths. This is reasonable, because also for a PAM alone a larger difference between the anti-resonance and resonance frequencies results in a higher bandwidth. The influence of the PAM-wall distance d_{w1} on the results in Fig. 3(b) is more complex. In general, a large value of d_{w1} leads to large bandwidths. But it can also be seen that the bandwidth of the wall with PAM increases slightly when $d_{w1} \to 0$. There is, however, a certain range of d_{w1} values for which the bandwidth is zero, regardless of the value for f_R/f_P. This zero bandwidth region can be attributed to a resonance of the multilayered system (which depends on the PAM-wall distance d_{w1}) cancelling out the anti-resonance of the PAM (which does not depend on the position of the PAM). The STL results shown in Fig. 4 for three different values of d_{w1} illustrate this phenomenon. For $d_{w1} = 2.5$ mm, a local STL minimum at a frequency slightly above the anti-resonance frequency $f_P = 300$ Hz can be observed which corresponds to a resonance of the combined system of wall, air gap, and PAM. When d_{w1} is increased to 15 mm, the stiffness of the air gap becomes smaller and the resonance frequency is reduced to nearly 300 Hz. The nearly coincidental anti-resonance and resonance frequencies cancel each other out, leading to the PAM having nearly no effect in front of the wall, despite of TL values of over 20 dB at 300 Hz for the PAM alone (red dashed curves). For $d_{w1} = 75$ mm (Fig. 4(c)), the resonance frequency is much lower than f_P and the bandwidth of the wall with PAM increases considerably.

An equation for predicting the critical PAM-wall distance d_{cr1} at which the pole-zero cancellation observed in Fig. 4(b) occurs can be deduced as follows: At the anti-resonance frequency f_P, the magnitude of the PAM effective surface mass density is much higher than that of the wall. Therefore, at f_P the PAM can be assumed to be a rigid wall. The configuration shown in Fig. 3(a) then changes to a wall with surface mass density m''_{w1} in front of a rigid wall with an air gap of thickness d_{w1}. This is equivalent to a panel resonator configuration for which the resonance frequency is given by $2\pi f_{panel} = \sqrt{\rho_0 c_0^2/(m''_{w1} d_{w1})}$ (13, p. 322). Letting $f_{panel} = f_P$ (i.e. coincidence of the panel resonance and anti-resonance of the PAM) and solving for the wall spacing results in the following expression for the critical wall spacing:

$$d_{cr1} = \frac{\rho_0 c_0^2}{4\pi^2 f_P^2 m_{w1}}. \tag{5}$$

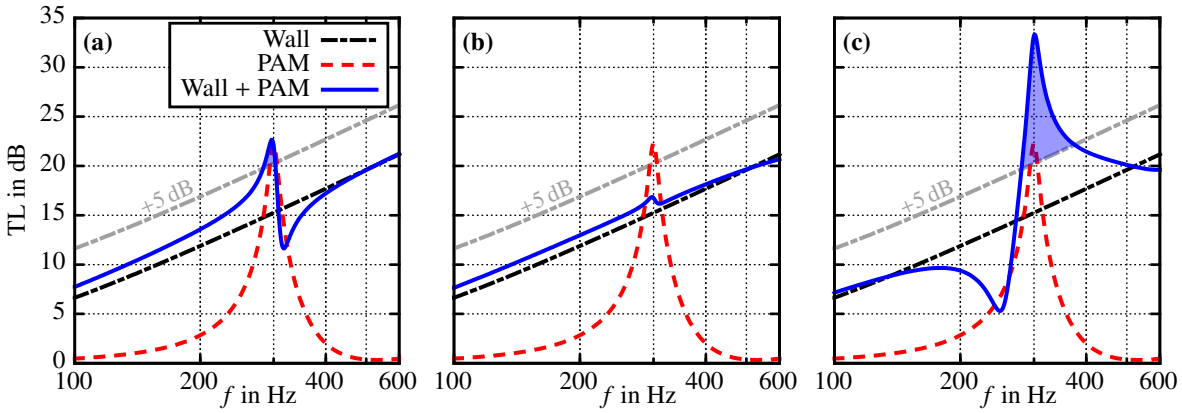

Figure 4 – Normal incidence sound transmission loss TL for a wall with a PAM (see Fig. 3) for different PAM-wall spacings d_{w1}. The shaded area indicates the frequency band with TL +5 dB above that of the wall only. (a) $d_{w1} = 2.5$ mm; (b) $d_{w1} = 15$ mm; (c) $d_{w1} = 75$ mm.

For the given PAM-wall configuration, Eq. (5) evaluates to $d_{cr1} = 15.9\,\text{mm}$ which is indicated as a dashed red line in Fig. 3 and marks the center of the zero bandwidth region.

The value of d_{cr1} in Eq. (5) depends only on the bulk modulus of the fluid, the PAM anti-resonance frequency f_P, and the surface mass density m''_{w1} of the base wall. Since these quantities typically are prescribed by requirements, it is difficult to adjust the critical wall spacing of a PAM-wall partition. Consequently, when designing such a partition, the distance d_{w1} should be chosen much smaller or much larger than the critical wall spacing d_{cr1} in order to achieve reasonably large bandwidths.

3.2 Double wall with PAM

The results for the relative +5 dB-bandwidth of the double wall with PAM (see Fig. 5(a) with baseline parameters given in Table 2) are shown in Fig. 5(b). In this case, the x-axis of Fig. 5(b) indicates a variation of the PAM position inside the double wall by varying d_{w1} from 0 to H. The mass-air-mass resonance frequency of the double wall without PAM (160 Hz) is significantly lower than the PAM anti-resonance frequency.

Like in the single wall configuration, a zero bandwidth region can again be identified at $d_{w1} = d_{cr1} = 15.9\,\text{mm}$ (corresponding to $d_{w1}/H = 0.106$). This can also be explained by the coincidence of the PAM anti-resonance frequency and the panel resonance frequency of the first wall at this value of d_{w1}. In addition to that, another zero bandwidth region can be seen in Fig. 5(b) for PAM positions close to the second wall. This can be explained in the same way as the first zero bandwidth region: At certain distances d_{w2} between the PAM and the second wall, the wall and the air layer can also exhibit a panel resonance if the PAM anti-resonance is equal to this second panel resonance frequency. Similar to the derivation of Eq. (5), the critical wall distance d_{cr2} (measured from wall #1) for coincidence with the second panel resonance of the double wall-PAM system can be obtained as

$$d_{cr2} = H - \frac{\rho_0 c_0^2}{4\pi^2 f_P^2 m_{w2}}. \tag{6}$$

For the investigated double wall configuration, $d_{cr2} = 123.5\,\text{mm}$ which is indicated as the second vertical red line in Fig. 5(b). This value corresponds well to the center of the second zero bandwidth region. Since both d_{cr1} and d_{cr2} are very close to each wall for this configuration, placing the PAM in the middle of the double wall is beneficial. Placing the PAM close to the second wall also results in large bandwidths, but the gradient is very steep and small variations in the PAM position (e.g. due to manufacturing tolerances) can lead to large changes in acoustical performance.

4. CONCLUSIONS

In the present contribution, the sound insulation performance of acoustic partitions with plate-like acoustic metamaterials (PAM) was evaluated using a simplified analytical model which represents the PAM by a set of five general parameters (m''_0, f_P, f_R, ζ_P, and ζ_R). The transfer matrix method was employed to estimate the sound transmission loss of multi-layered partitions containing PAM layers. The proposed model was

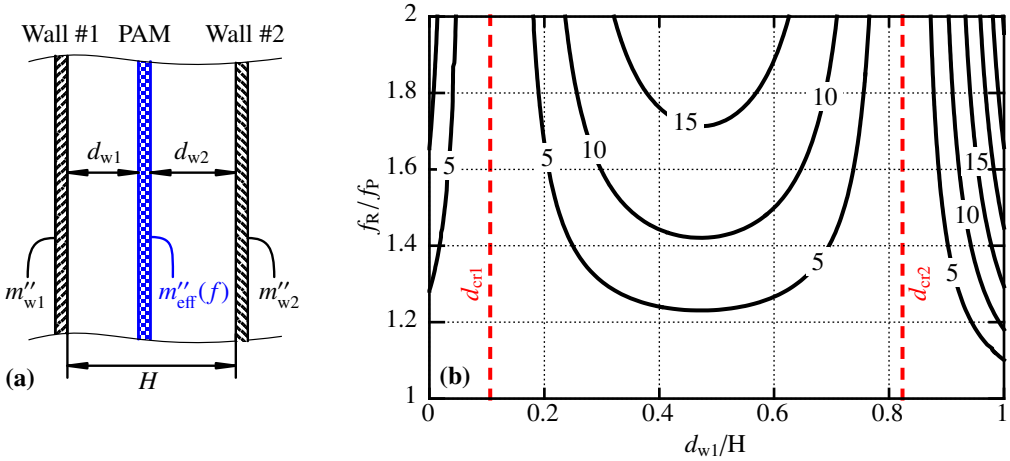

Figure 5 – Sound insulation performance of a double wall with PAM layer. (a) Schematical representation of the configuration; (b) +5 dB-bandwidth (in %) for different PAM positions d_{w1}/H and relative PAM resonance frequencies f_R/f_P (baseline parameters given in Table 2).

validated using numerical simulations of different PAM unit cell designs and laboratory measurements of a 50 cm × 50 cm plate model under diffuse field excitation.

By applying the model to single and double wall partition designs with an additional PAM layer, the influence of the PAM resonance frequency as well as the distance between the wall(s) and the PAM on the sound insulation enhancement of the partition could be systematically investigated. It was found that if the PAM is placed at certain critical distances with respect to the wall(s), the anti-resonance of the PAM can be practically nullified due to the panel resonance of a wall being coincidental with the PAM anti-resonance frequency. Simple expressions could be derived for these critical distances using the proposed generalized PAM model. These distances depend only on the fluid bulk modulus, the wall masses, and the PAM anti-resonance frequency. In the design of acoustic partitions with PAM the metamaterial layers must be positioned as far away from these critical distances as possible to achieve the highest performance.

Additionally, the five parameter model for the PAM can be applied to simplify the early design of such partitions: Instead of committing to a specific PAM design in the first step, the partition can be designed using the five general PAM parameters without knowing the exact details of the metamaterial. Once the desirable parameters of the PAM have been determined, a suitable metamaterial design fulfilling these (and other) requirements can be selected from the different realizations available in the literature. This novel approach for the design of acoustic partitions with metamaterials could support the application of acoustic metamaterials in practical noise control problems.

ACKNOWLEDGEMENTS

This work has been performed under the framework of the German-Canadian joint research project New Acoustic Insulation Metamaterial Technology for Aerospace (NAIMMTA), funded by the Federal Ministry of Education and Research (grant number: 03INT504AB). The financial support is gratefully acknowledged by the authors.

REFERENCES

1. Cummer SA, Christensen J, Alù A. Controlling sound with acoustic metamaterials. Nat Rev Mater. 2016;1:16001.
2. Yang Z, Mei J, Yang M, Chan NH, Sheng P. Membrane-Type Acoustic Metamaterial with Negative Dynamic Mass. Phys Rev Lett. 2008;101(20):204301.
3. Kurtze G. Light-weight walls with high transmission loss. Acta Acust united Ac. 1959;9(6):441–5.
4. Weber L, Kaltbeitzel B, Maysenhölder W. Verbesserung der Schalldämmung von leichten Ständerwänden bei tiefen Frequenzen [Improvement of the sound transmission loss of lightweight stud walls at low frequencies]. Stuttgart, Germany: Fraunhofer IRB Verlag; 2018.
5. Langfeldt F, Gleine W. Improved Sound Transmission Loss of Glass Wool With Acoustic Metamaterials. Proc 26th ICSV; 7–11 July 2019; Montréal, Canada 2019.
6. Xiao Y, Wen J, Wen X. Sound transmission loss of metamaterial-based thin plates with multiple subwavelength arrays of attached resonators. J Sound Vib. 2012;331(25):5408–23.
7. Claeys C, Deckers E, Pluymers B, Desmet W. A lightweight vibro-acoustic metamaterial demonstrator: Numerical and experimental investigation. Mech Syst Signal Process. 2016;70-71:853–80.
8. Langfeldt F, Gleine W, von Estorff O. Enhancing the low-frequency noise reduction of a double wall with membrane-type acoustic metamaterials. Proc Inter-Noise 2016; 21–24 August 2016; Hamburg, Germany 2016. p. 7551–62.
9. De Melo Filho N, Belle LV, Claeys C, Deckers E, Desmet W. Dynamic mass based sound transmission loss prediction of vibro-acoustic metamaterial double panels applied to the mass-air-mass resonance. Journal of Sound and Vibration. 2019;442:28–44.
10. Allard JF, Atalla N. Propagation of Sound in Porous Media: Modelling Sound Absorbing Materials. 2nd ed. Chichester: John Wiley & Sons; 2009.
11. Allard J, Champoux Y. New empirical equations for sound propagation in rigid frame fibrous materials. J Acoust Soc Am. 1992;91(6):3346–53.
12. Bonfiglio P, Pompoli F, Lionti R. A reduced-order integral formulation to account for the finite size effect of isotropic square panels using the transfer matrix method. J Acoust Soc Am. 2016;139(4):1773–83.
13. Bies DA, Hansen CH. Engineering Noise Control: Theory and Practice. 4th ed. London, United Kingdom: Spon Press; 2009.